Note on microperforated panel model using equivalent-fluid-based absorption elements

Okuzono, Takeshi
Nitta, Takao
Sakagami, Kimihiro

(Citation)
Acoustical Science and Technology,40(3):221-224

(Issue Date)
2019-05-01

(Resource Type)
journal article

(Version)
Version of Record

ACOUSTICAL LETTER

Note on microperforated panel model using equivalent-fluid-based absorption elements

Takeshi Okuzono*, Takao Nitta and Kimihiro Sakagami

Environmental Acoustic Laboratory, Department of Architecture, Graduate School of Engineering, Kobe University, 1–1 Rokkodai, Nada, Kobe, 657–8501 Japan

(*Received 17 December 2018, Accepted for publication 5 January 2019*)

Keywords: FEM, MPP, Equivalent fluid model
PACS number: 43.55.Ka, 43.55.Dt, 43.55.Ev [doi:10.1250/ast.40.221]

1. Introduction

A microperforated panel (MPP) is a thin panel with submillimeter holes below a 1% perforation ratio [1]. MPPs satisfy requirements for both sound absorptivity and designability. Therefore, they are useful as attractive sound-absorbing structures for comfortable acoustical design in built environments. In recent years, various numerical approaches [2–9] have been applied to predict absorption characteristics of MPP absorbers with complex configurations. Among them, a simple approach uses equivalent-fluid-based absorption finite elements (FEs) [2,7,9]. Two methods are used in the approach: one addresses the MPP itself as a rigid frame equivalent fluid [2]; the other addresses only air inside its holes as an equivalent fluid [7,9]. The present investigation addresses the latter method. The advantage of the latter method over the former method is that it can model MPP absorbers with nonuniform hole arrangements or different hole diameters. Additionally, it is easier to apply than approaches using the frequency domain linearized Navier–Stokes solver [6] and computational fluid dynamics [3,5]. Nevertheless, the accuracy of the approach using absorption FEs inside a hole has been insufficiently verified. In this paper, we describe its accuracy in comparison with a theoretical model based on the Guo model [10], particularly addressing the acoustic impedance of MPPs.

2. Theory

2.1. Transfer impedance model of MPP

The various transfer impedance models of a rigid-frame MPP have different resistive end correction treatments to describe the effects of surface resistance. In this paper, we use the Guo model [10], which can include various resistive end correction treatments. The transfer impedance Z_t of an MPP is represented as

$$Z_t = \frac{j\omega\rho_e t}{\varepsilon} + \frac{\alpha 2R_s}{\varepsilon} + \frac{j\omega\rho_0\delta}{\varepsilon}. \tag{1}$$

In Eq. (1), the first term represents the effect of viscous loss inside a hole. Also, j is an imaginary unit, ω the angular frequency, ρ_e the complex effective density inside a hole that incorporates the viscous loss, t the panel thickness, and ε the perforation ratio. For MPPs with circular holes, the complex effective density is given as

$$\rho_e = \frac{\rho_0}{1 - \dfrac{2}{\sqrt{-j}}\dfrac{J_1(s\sqrt{-j})}{J_0(s\sqrt{-j})}}, \quad s = r\sqrt{\frac{\omega\rho_0}{\eta}}, \tag{2}$$

where J_0 and J_1 respectively represent Bessel functions of the first kind on the zeroth and first orders, r is the hole radius, η the air viscosity, and ρ_0 the air density. The second term of Eq. (1) expresses the resistive end correction by the surface resistance $R_s = \sqrt{2\eta\rho_0\omega}/2$, and α is a coefficient. Table 1 presents α values for some models. The third term of Eq. (1) expresses the reactive end correction by the end correction factor δ, showing the effect of added mass at the neck.

The effective density given by Eq. (2) can be replaced by the following for holes with an arbitrary cross-sectional shape [11]:

$$\rho_e = \rho_0\left(1 + \frac{\sigma\phi}{j\omega\rho_0}G_c(s)\right), \tag{3}$$

$$G_c(s) = -\frac{s}{4}\sqrt{-j}\frac{J_1(s\sqrt{-j})}{J_0(s\sqrt{-j})} \Bigg/ \left[1 - \frac{2}{s\sqrt{-j}}\frac{J_1(s\sqrt{-j})}{J_0(s\sqrt{-j})}\right], \tag{4}$$

where $\sigma\phi$ is the flow resistivity, which depends on the cross-sectional shape of the hole, e.g., $\sigma\phi = 8\eta/\bar{r}^2$ for a circular hole and $\sigma\phi = 7\eta/\bar{r}^2$ for a square hole [11]. The hydraulic radius $\bar{r}$ is defined as $\bar{r} = 2S/l$, where l represents the hole perimeter and S stands for the cross-sectional area of the hole. With the shape-dependent factor $c = \sqrt{8\eta/(\sigma\phi)}/\bar{r}$, the parameter s is given as

$$s = c\sqrt{\frac{8\omega\rho_0}{\sigma\phi}}. \tag{5}$$

2.2. Surface impedance of single-leaf MPP absorber

A single-leaf MPP absorber is the most classical MPP absorber, in which an MPP is placed in front of a rigid-backed air cavity. The surface impedance Z_{surf} is expressed as [1]

$$Z_{surf} = Z_t - j\rho_0 c_0 \cot(k_0 L), \tag{6}$$

where c_0, k_0, and L respectively represent the speed of sound in air, the wavenumber of air, and the backing cavity depth.

2.3. Microperforation model using absorption FEs

In absorption FEs based on an equivalent fluid model, the air inside porous media is modeled at a macroscopic scale as

*e-mail: okuzono@port.kobe-u.ac.jp

Table 1 Some α values for resistive end correction in various transfer impedance models, where f represents the frequency.

Model	α
Maa [1]	0.5
Guo [10]	2.0 (for rounded holes) 4.0 (for sharp-edged holes)
Bolton and Kim [3]	$\beta f^{-0.5}$ with $\beta = (14.1 - 0.059\varepsilon)\frac{t}{d} + 117$

an equivalent fluid with complex effective density ρ_e and complex bulk modulus K_e that incorporates viscothermal loss. Sound propagation in the medium is described by the following Helmholtz equation:

$$\nabla^2 p + \left(\omega\sqrt{\frac{\rho_e}{K_e}}\right)^2 p = 0. \tag{7}$$

As described herein, sound propagation in a microperforation is explained by the equation above with the effective density given by Eq. (3) or with a modified effective density, as presented in a later section of this paper. The bulk modulus K_e with the dissipative effect of heat conduction is given as [11]

$$K_e = \gamma P_0/(\gamma - [\gamma - 1]F(B^2\omega)), \tag{8}$$

$$F(B^2\omega) = 1 \Big/ \left[1 + \frac{\sigma\phi}{jB^2\omega\rho_0} G_c(Bs)\right], \tag{9}$$

where γ is the specific heat ratio, P_0 the atmospheric pressure, and B^2 the Prandtl number.

3. Numerical experiments

In this section, single-leaf MPP absorbers with circular and square holes were modeled using the absorption FEs. The surface impedance and the normal incidence absorption coefficient α_0 were calculated using a transfer function method with the impedance tube model in Fig. 1. Sound fields except those for the microperforation were modeled using a conventional lossless Helmholtz equation, and were coupled with the sound field inside the microperforation by the continuity conditions in terms of the sound pressure and particle velocity on the contact surface. The accuracy of FEM results was evaluated by comparing with the theory using

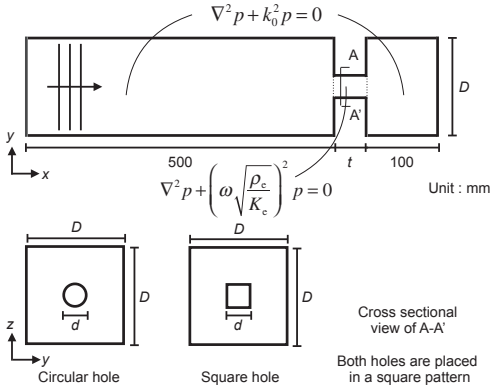

Fig. 1 Impedance tube model with a single-leaf MPP absorber used for FE analysis.

Table 2 Specifications of MPP with circular and square holes.

	Circular hole	Square hole
Hole diameter, d	1.0 mm	1.0 mm
Panel thickness, t	1.0 mm	1.0 mm
Pitch, D	9.0 mm	17.0 mm
Perforation ratio, ε	0.9696%	0.3460%

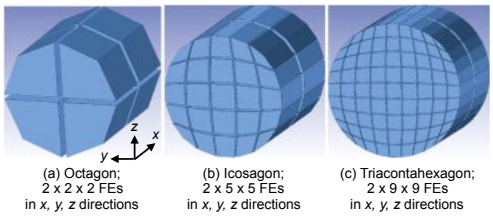

Fig. 2 Spatial discretization in a circular hole.

Eq. (6). Here, ρ_e given by Eq. (3) was used for both theory and FE analyses. In the theory, the α value when modeling surface resistance is 0.5. Table 2 presents the geometrical parameters of the MPP for the circular and square holes. The sound field was discretized by eight-node hexahedral linear FEs. In the tube and backing air cavity, the maximum element size is 5 mm. The mesh has a spatial resolution of 68 elements per wavelength at 1 kHz, which is sufficient for a general acoustic analysis. The circular hole was modeled using polygonal approximations as presented in Fig. 2. Also, three levels of approximation, i.e., octagon, icosagon, and triacontahexagon, were tested because the approximation level of the shape affects the resulting accuracy. The maximum element size inside the holes is 0.5 mm, which also has sufficient spatial resolution. This is also true for the square hole. Considering the hole arrangements shown in Fig. 1, in theory, the end correction factors for a circular hole δ_c and a square hole δ_s are given as [12]

$$\delta_c = 0.85d(1 - 1.13\varepsilon^{1/2} - 0.09\varepsilon + 0.27\varepsilon^{3/2}), \tag{10}$$

$$\delta_s = 0.85d(1 - 1.33\varepsilon^{1/2} - 0.07\varepsilon + 0.40\varepsilon^{3/2}). \tag{11}$$

3.1. Results and discussion

Figure 3 presents comparisons of surface impedance and α_0 between the theory and FEM for the circular hole. The resistance of the surface impedance in the FEM results increasingly underestimates the theoretical value with increasing approximation level of the circular shape. The reactance shifts to a frequency higher than the theoretical value. FEM using ρ_e from Eq. (3) does not incorporate surface resistance effects, which is the reason for the discrepancy from the theoretical resistance. The discrepancy in reactance is attributable to differences in the end correction factors between the theory and FEM. In fact, FEM shows a higher resonance frequency than the theory, meaning that the added mass at the neck was underestimated. Although in FEM reactive end correction is considered naturally because all sound fields are analyzed, the mesh resolution (5 mm maximum) is higher than theoretical end correction value

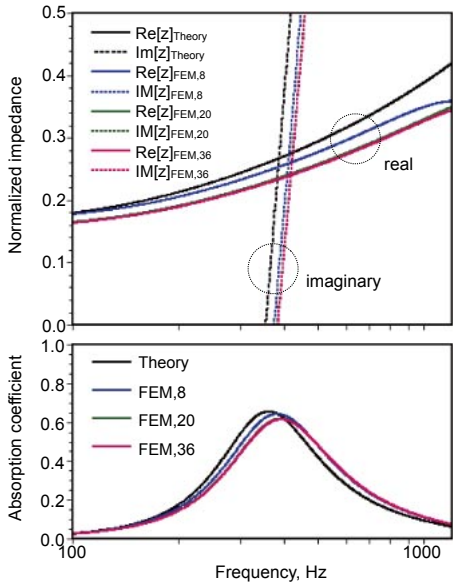

Fig. 3 Comparison of $Z_{\mathrm{surf}}/\rho_0 c_0$ (upper) and α_0 (lower) between theory and FEM for the circular hole. FEM,8, FEM,20, and FEM,36 respectively represent results for octagon, icosagon, and triacontahexagon approximations.

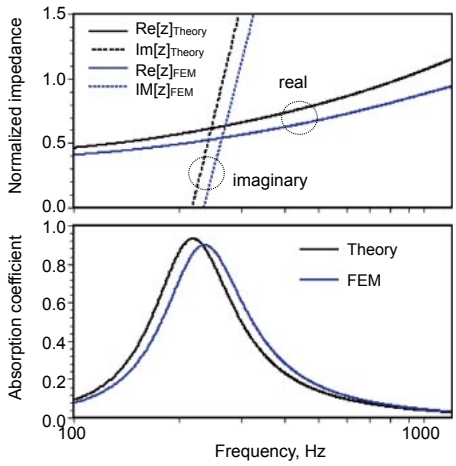

Fig. 4 Comparison of $Z_{\mathrm{surf}}/\rho_0 c_0$ (upper) and α_0 (lower) between theory and FEM for the square hole.

$\delta_c = 0.7549$ mm. Therefore, the discrepancy is attributed to the insufficient spatial resolution of the mesh used here, although the resolution is sufficient for general acoustic analyses. Figure 4 shows that the results for the square hole exhibit the same tendency as those for the circular hole.

4. Introduction of modified effective density

A modified effective density $\tilde{\rho}_e$ is introduced to address the surface resistance effect in FEM. $\tilde{\rho}_e$, which includes the surface resistance effect in the effective density ρ_e, is expressed as

$$\tilde{\rho}_e = \rho_0 \left(1 + \frac{\sigma\phi}{j\omega\rho_0} G_c(s) + \frac{\alpha 2 R_s}{j\omega t \rho_0} \right). \tag{12}$$

The transfer impedance given by Eq. (1) is described as follows using $\tilde{\rho}_e$:

$$Z_t = \frac{j\omega\tilde{\rho}_e t}{\varepsilon} + \frac{j\omega\rho_0\delta}{\varepsilon}. \tag{13}$$

The modified effective density approach is based on an idea reported by Kim and Yoon [7]. They presented an effective density with a modified tortuosity in the Johnson-Champoux-Allard (JCA) model. The tortuosity in the JCA model was modified so that both the resistive and reactive end correction effects fit the Beranek–Ingard model. Our definition of $\tilde{\rho}_e$ is based on the Guo model with the effective density given by Eq. (3). It can accommodate the use of various surface resistance treatments and various hole shapes. A further difference is that only the surface resistance effect is included in $\tilde{\rho}_e$. As described later, reactive end correction should not be included. As a reference, the MPP itself is modeled as a rigid frame equivalent fluid medium based on the Guo model with the effective density ρ_{eq} and bulk modulus K_{eq} as

$$\rho_{eq} = \frac{\rho_0}{\varepsilon} \left(1 + \frac{\sigma\phi}{j\omega\rho_0} G_c(s) + \frac{\alpha 2 R_s}{j\omega t \rho_0} + \frac{\delta}{t} \right) \tag{14}$$

$$K_{eq} = K_e/\varepsilon. \tag{15}$$

However, the absorption FEs assume isotropy. For this reason, the expression above must be used carefully.

4.1. Improved numerical results and discussion

Figures 5 and 6 respectively present results obtained using the modified effective densities $\tilde{\rho}_e$ for circular and square holes. For the circular hole, FEM using the $\tilde{\rho}_e$ is in better agreement with the theoretical resistance when the

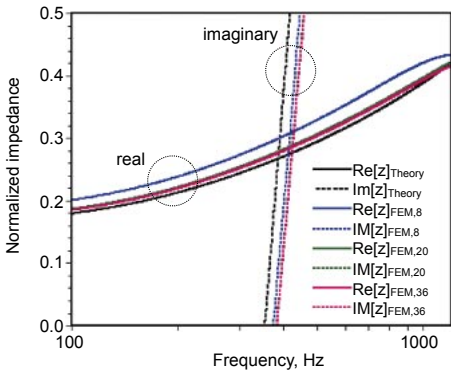

Fig. 5 Comparison of $Z_{\mathrm{surf}}/\rho_0 c_0$ between theory and FEM using $\tilde{\rho}_e$ for the circular hole.

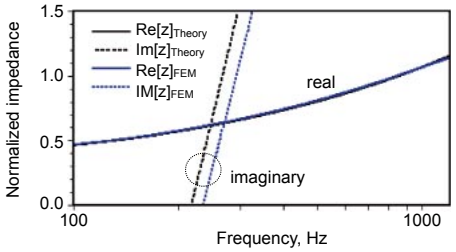

Fig. 6 Comparison of $Z_{\mathrm{surf}}/\rho_0 c_0$ between theory and FEM using $\tilde{\rho}_e$ for the square hole.

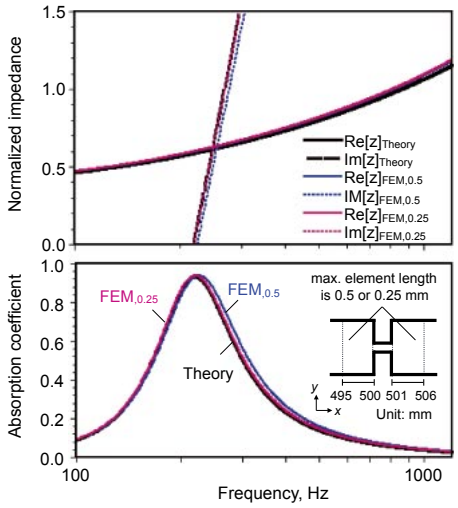

Fig. 7 Results obtained using finer meshes near the square hole. $Z_{\mathrm{surf}}/\rho_0 c_0$ (Upper) and α_0 (Lower) between theory and FEM using $\tilde{\rho}_{\mathrm{e}}$. FEM,0.5 and FEM,0.25 respectively represent results obtained using FE meshes with 0.5 mm and 0.25 mm elements near the perforation.

approximation level of the circular shape becomes higher. A slight discrepancy exists even for the triacontahexagon approximation. Therefore, a higher approximation is necessary. The agreement in the resistance is also good in the case of a square hole, which does not include errors in the hole shape. This result demonstrates the effectiveness of using $\tilde{\rho}_{\mathrm{e}}$.

Furthermore, Fig. 7 presents results obtained using finer meshes, which were used to improve the agreement in the reactance by resolving the sound field near the perforation more precisely. As the figure shows, we used two meshes for the square-hole case, and the sound field near the perforation, which is the regions of 495–500 mm and 501–506 mm in the x direction, was discretized by smaller elements with maximum lengths of 0.5 mm and 0.25 mm. For the remaining sound field the maximum element size is 5 mm. Results showed that the use of finer meshes engenders better agreement with the theory for both the reactance and α_0. This tendency is also observed for the circular-hole case. The theoretical resonance frequency is 218 Hz. The frequencies are, respectively, 224 Hz and 219 Hz for the FEM results obtained using meshes with 0.5 mm and 0.25 mm elements.

5. Conclusions

In this paper, we presented the accuracy of the MPP model using absorption FEs inside a hole in comparison with the corresponding theory based on the Guo model. Results demonstrated that the use of a modified effective density, which includes the surface resistance effect, is necessary to obtain better agreement with the theoretical resistance. Additionally, the use of a sufficiently fine mesh near the perforation is required to precisely reproduce the added-mass effect at the neck. Otherwise, the added mass is underestimated. For circular holes, a high level of approximation of the circular shape is important to evaluate the theoretical resistance correctly when one uses linear hexahedral FEs and the modified effective density. More detailed investigations conducted under various conditions remain as goals for future research.

Acknowledgment

This work was supported by JSPS KAKENHI Grant No. 17K14771.

References

[1] D. Y. Maa, "Potential of microperforated panel absorber," *J. Acoust. Soc. Am.*, **104**, 2861–2866 (1998).
[2] K. Hou and J. S. Bolton, "Finite element models for microperforated panels," *Proc. Inter·noise 2009*, 9 pages (2009).
[3] J. S. Bolton and N. Kim, "Use of CFD to calculate the dynamic resistive end correction for microperforated materials," *Acoust. Aust.*, **38**, 134–139 (2010).
[4] C. Wang and L. Huang, "On the acoustic properties of parallel arrangement of multiple micro-perforated panel absorbers with different cavity depths," *J. Acoust. Soc. Am.*, **130**, 208–218 (2011).
[5] T. Herdtle, J. S. Bolton, N. N. Kim, J. H. Alexander and R. W. Gerdes, "Transfer impedance of microperforated materials with tapered holes," *J. Acoust. Soc. Am.*, **134**, 4752–4762 (2013).
[6] J. Carbajo, J. Ramis, L. Godinho, P. A. Mendes and J. Alba, "A finite element model of perforated panel absorbers including viscothermal effects," *Appl. Acoust.*, **90**, 1–8 (2015).
[7] K. H. Kim and G. H. Yoon, "Absorption performance optimization of perforated plate using multiple-sized holes and a porous separating partition," *Appl. Acoust.*, **120**, 21–37 (2017).
[8] T. Okuzono and K. Sakagami, "A frequency domain finite element solver for acoustic simulations of 3D rooms with microperforated panel absorbers," *Appl. Acoust.*, **129**, 1–12 (2018).
[9] J. Carbajo, J. Ramis, L. Godinho and P. A. Mendes, "Assessment of methods to study the acoustic properties of heterogeneous perforated panel absorbers," *Appl. Acoust.*, **133**, 1–7 (2018).
[10] Y. Guo, S. Allam and M. Abom, "Micro-perforated plates for vehicle applications," *Proc. Inter·noise 2008*, 19 pages (2008).
[11] J. F. Allard and N. Atalla, "Sound propagation in cylindrical tubes and porous materials having cylindrical pores," in *Propagation of Sound in Porous Media: Modeling Sound Absorbing Materials*, 2nd ed. (John Wiley & Sons, Chichester, 2009), Chap. 4, pp. 45–72.
[12] T. J. Cox and P. D'Antonio, "Resonant absorbers," in *Acoustic Absorbers and Diffusers: Theory, Design and Application*, 3rd ed. (CRC Press, Boca Raton, 2017), Chap. 7, pp. 225–264.